VELOCITY PHASE SPACE STUDIES OF ION DYNAMICS IN THE VASIMR ENGINE

Edgar A. Bering, III*, University of Houston, Houston, TX,
Franklin R. Chang Díaz†, Jared P. Squire‡, Timothy W. Glover§,
Advanced Space Propulsion Laboratory, JSC / NASA, Houston, TX,
Roger D. Bengtson¶, University of Texas at Austin, Austin, TX,
and Michael Brukardt#, University of Houston, Houston, TX

ABSTRACT

The Variable Specific Impulse Magnetoplasma Rocket (VASIMR) is a high power, radio frequency-driven magnetoplasma rocket, capable of Isp/thrust modulation at constant power. The physics and engineering of this device have been under study since 1980. The plasma is produced by an integrated helicon discharge. However, the bulk of the plasma energy is added in a separate downstream stage by ion cyclotron resonance heating (ICRH.) Axial momentum is obtained by the adiabatic expansion of the plasma in a magnetic nozzle. Exhaust variation in the VASIMR is primarily achieved by the selective partitioning of the RF power to the helicon and ICRH systems, with the proper adjustment of the propellant flow. However, other complementary techniques are also being considered. A NASA-led, research effort, involving several teams in the United States, continues to explore the scientific and technological foundations of this concept. The research is multifaceted and involves theory, experiment, engineering design, mission analysis, and technology development. Experimentally, high density, stable plasma discharges have been generated in Helium, Hydrogen, Deuterium, Argon and Xenon. Theoretically, the dynamics of the magnetized plasma are being studied from kinetic and fluid approaches. Plasma acceleration by the magnetic nozzle and subsequent detachment has been demonstrated in numerical simulations. These results are presently undergoing experimental verification. Plasma properties of the helicon discharge and exhaust plasma have been measured under a variety of conditions. This paper will review the ion energy and velocity measurments obtained in 2002-2004 in a continuing series of performance optimization and design development studies and will outline plan and strategies for continued research.

INTRODUCTION

The VASIMR engine has three major subsystems, the injection stage, the heating stage and the nozzle[1,2,3,4,5]. The details of the engine and its design principles were presented in the previous paper[5]. The use of a separate helicon discharge[6,7] injection system has allowed us to optimize our system for maximum power efficiency over a wide range of gas flow rates. The heating system feeds energy in the form of a circularly polarized RF signal tuned to the ion cyclotron frequency. ICRH heating has been chosen because it transfers energy directly and primarily to the ions, which maximizes the efficiency of the engine, as has been demonstrated in linear devices[8,9]. In the present small-scale test version, the ions make one pass through the ICRH antenna. The system also features a magnetic nozzle, which accelerates the plasma

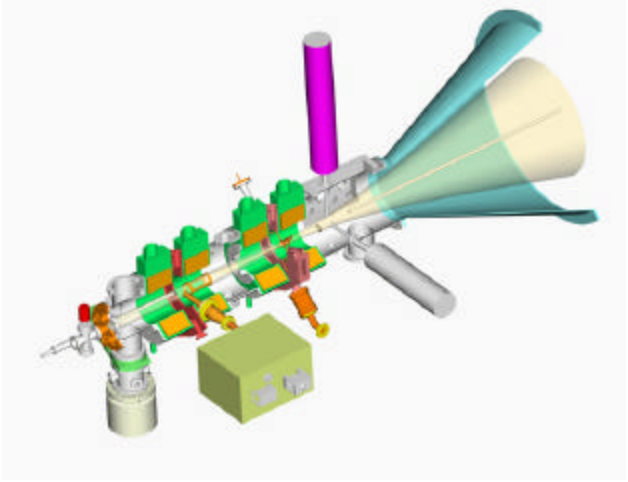

Figure 1: The VASIMR System

* Professor, Physics and Electrical and Computer Engineering, eabering@uh.edu
† NASA Astronaut, ASPL Director
‡ Senior Research Scientist, Muniz Engineering
§ Research Scientist, Muniz Engineering , Inc.
¶ Professor, Physics, University of Texas
# Research Assistant, Physics, UH

particles by converting their azimuthal energy into axial flow. The detachment of the plume from the field takes place mainly by the loss of adiabaticity and the rapid increase of the local plasma β, defined as the local ratio of the plasma pressure to the magnetic pressure. A schematic representation of the present laboratory experiment is shown in Figure 1.

A NASA-led, multifaceted research effort, involving several teams in the United States, continues to explore the scientific and technological foundations of this concept, and its extrapolation as a high power, in space propulsion system[4,10]. Experimentally, two major facilities are investigating plasma performance. Both have obtained attractive results with hydrogen and helium, the two propellants of choice. In helium, densities of 10^{19} m^{-3} have been obtained at frequencies near the lower hybrid resonance[11]. Slightly lower densities, in range of 10^{18} m^{-3} have been obtained with hydrogen. Further investigations using deuterium, as well as other gas mixtures are being conducted.

A laboratory version of a 25 kW proof of concept VASIMIR engine has been under development and test at NASA-JSC for several years[4,12,13]. Available plasma diagnostics include a triple probe, a Mach probe, a bolometer, a television monitor, an H-α photometer, a spectrometer, neutral gas pressure and flow measurements, several gridded energy analyzers (retarding potential analyzer or RPA)[4], a surface recombination probe system, an emission probe, a directional, steerable RPA and other diagnostics. Reciprocating Langmuir and Mach probes are the primary plasma diagnostics. The Langmuir probe[14] measures electron density and temperature profiles while the Mach probe[15,16] measures flow profiles. Together this gives total plasma particle flux. An array of thermocouples provides a temperature map of the system. The Langmuir probe has four molybdenum tips that are biased as a triple probe, with an extra tip for measuring electrostatic fluctuations[13]. The Mach probe has two molybdenum tips biased in ion saturation, one upstream and one downstream of a stainless steel separator[14,15].

MAGNETIC CONFIGURATION IN VASIMR

The VASIMR system consists of three major magnetic cells, denoted as "forward," "central," and "aft". A magnet configuration example (related to a 24 kW VASIMR thruster conceptual design) and the corresponding magnetic field profile are shown in Figure 2. The forward end-cell provides the injection of the neutral gas to be ionized by electromagnetic waves that are produced by a helicon antenna. In the central-cell, the plasma is also electro-magnetically heated by waves operating near the Ion-Cyclotron Resonant Frequency (ICRF). The aft end-cell ensures that the plasma will efficiently detach from the magnetic field to provide propulsion through a highly directed exhaust stream. This magnetic configuration allows the plasma exhaust to be guided and controlled over a wide range of plasma energies and densities. In Figure 2, the forward end-cell is located at $z < 0.7$ *(m)*, the central cell at $0.7 < z < 1$ and the aft end-cell is at $1 < z$.

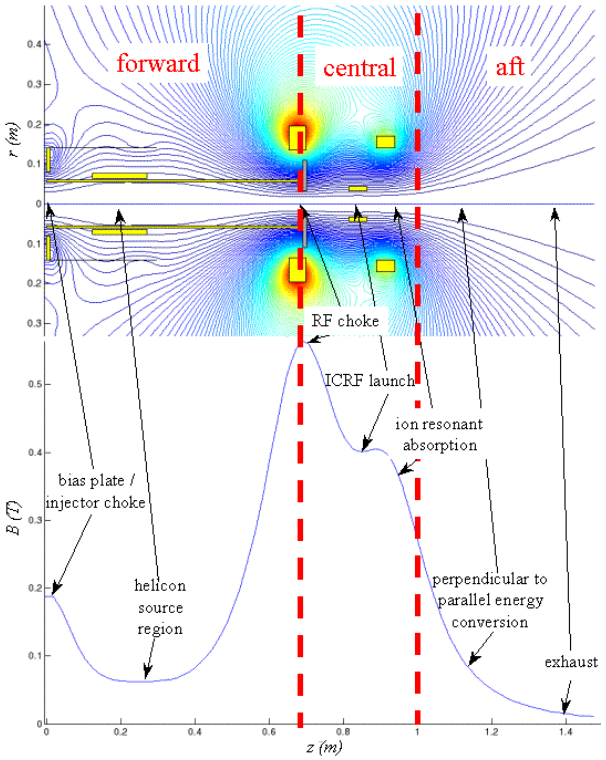

Figure 2: Geometry and magnetic field configuration for 24 kW VASIMR thruster.

RETARDING POTENTIAL ANALYZER

Retarding potential analyzer (RPA) diagnostics have been installed to measure the accelerated ions[4]. The present RPA is a planar ion trap located ~40 cm downstream from the plane of the triple and Mach probes, which corresponds to a factor of 8 reduction in the magnetic field strength. The grids are 125-wire/in nickel mesh, spaced 1 mm apart with Macor spacers. The opening aperture is 1 cm in diameter, nominally centered on the plasma beam. A four-grid configuration is used, with entrance attenuator, electron suppressor, ion

analyzer and secondary suppressor grids.

The interpretation of RPA output data in terms of ion energy requires an accurate knowledge of plasma potential (V_p). On University of Houston (UH) RPA plots, the 0 of the retarding potential scale is set to V_p as shown in Figure 3, instead of to chamber ground. Thus, the sweep scale can be read directly as ion energy in eV. When available, data from an RF compensated swept Langmuir probe provided by Los Alamos National Laboratory are used to determine V_p (*M. Light*, personal communication, 2003). When other V_p data are not available, plasma potential is assumed to be the value at which dI/dV first significantly exceeds 0, which usually agrees with the LANL probe value within the error bars. This value is typically ~+30-50 V with respect to chamber ground. The operator biases the body and

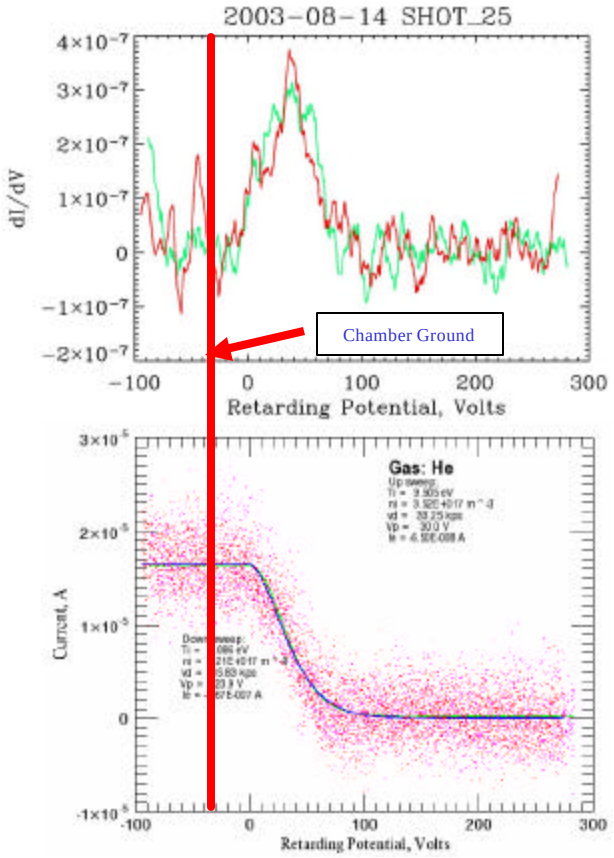

Figure 3. A sample shot of RPA data, showing relationship of chamber ground to plasma potential.

entrance aperture of the RPA to this value. The solid lines on the raw data plots are the results of least squares fits of drifting Maxwellians to the up and down sweeps.

We can find an upper limit to RF smearing of the current-voltage characteristic of the RPA by examining T_i estimates from the coldest plasma shots obtained. The coldest ion temperature observed with ICRF off was 3.4 eV observed with a very high gas flow. The coldest ion temperature during an ICRF on shot was ~5.8 eV, observed when the magnetic field strength in magnet 3 was lowered, moving the resonance region upstream of the antenna. These temperatures represent experimental upper limits on the RF contamination of ion temperature estimates.

EXPERIMENTAL RESULTS

Starting in 2000, we have performed a series of experiments on the VASIMR apparatus with several objectives, to explore the parameter space that optimizes helicon operation, to learn to operate the apparatus in high power modes and to demonstrate ICRF heating (ICRH) of the plasma. In the past year, we have increased the diameter of the helicon discharge to 9 cm.

For example, we have studied the effect of the strength of the mirror magnet in the ICRH region on the performance of the helicon without any ICRH heating. The results of these experiments are shown in Figures 4 and 5. In looking at these figures, one point must be made regarding the comparison of the RPA and Mach probe data. When the RPA and the Mach probe are put in the same plane, which was done in 1999, the inferred ion bulk flow speeds agree within 20%, as do the forward vs. backward saturation current ratios. When the RPA is placed ~40 cm downstream from the Mach probe, the inferred speeds increase. We attribute this apparent acceleration to a combination of adiabatic (magnetic mirror) acceleration and ambipolar electrostatic forces. The inverse relationship between thrust and specific impulse shown in Figure 5 is an illustration of the constant power-throttling concept (CPT).

We also observe an acceleration of the plasma flow past the high magnetic mirror field. The Mach probe used to measure data downstream of the magnetic mirror, for Figure 4, was moved to a location upstream of the mirror field. Figure 6 shows the magnetic field axial profile and the two locations for the Mach probe measurements. The Mach number measured upstream is half that measured downstream, Figure 7.

One of the most significant results of the light ion helicon development effort in the past year has been the achievement of ~100% propellant utilization. This improvement in ionization efficiency of the helicon discharge was obtained by improving confinement the injected neutral propellant to the interior of the discharge by means of a gas baffle and choke arrangement. Figure 8 shows the total ion output of the discharge plotted as a function of input gas flow. The different curves

correspond to different helicon RF levels. The data show that the ion flux is proportional to input gas flux for all but the lowest power level, until a power level dependent saturation value is reached.

We have also begun to investigate the details of the velocity space distribution function in the plasma, as shown in Figure 9. This figure was obtained from a set of measurements taken with a plain cylindrical quartz tube in the helicon, with no gas baffling or choke installed.

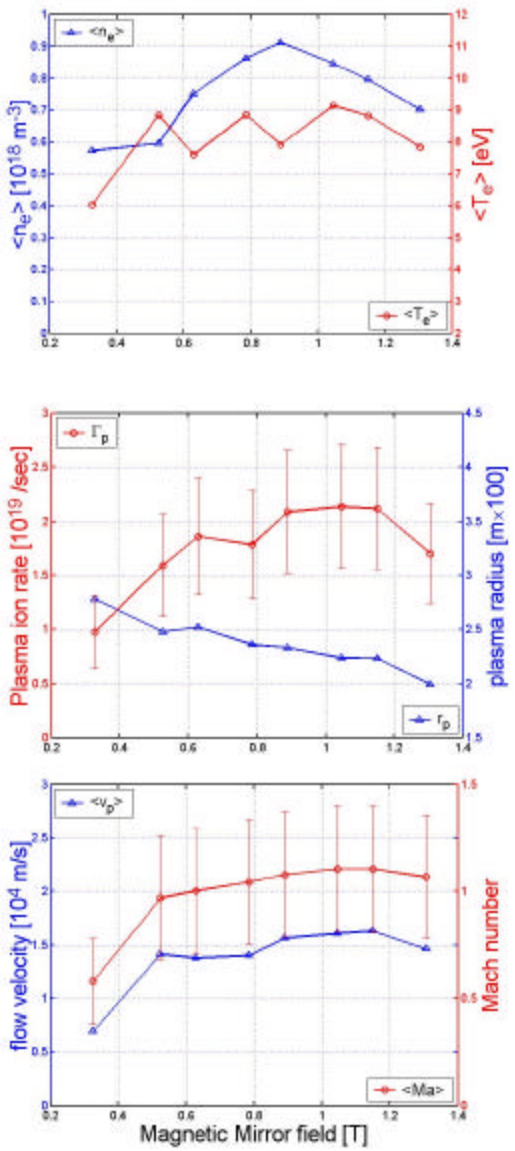

Figure 4. Triple and Mach probe data for a series of shots with the mirror field varying and all other parameters held fixed. Helicon RF input was 25 MHz with 3 kW. The error bars represent the difference in Mach probe theory models.

The distribution shown in Figure 9 shows a peak of ~40-45 km/s. The peak is not confined to a narrow axial beam, but is spread out in a ring-like distribution with a broad maximum covering most of the forward hemisphere. This ring continues with reduced intensity all the way around to 180°. We interpret this ring feature as clear evidence for a substantial amount of pitch angle scattering during the exhaust process. We believe that this pitch angle scattering was driven by the presence of ion whistlers or possibly ion-neutral collisions. The

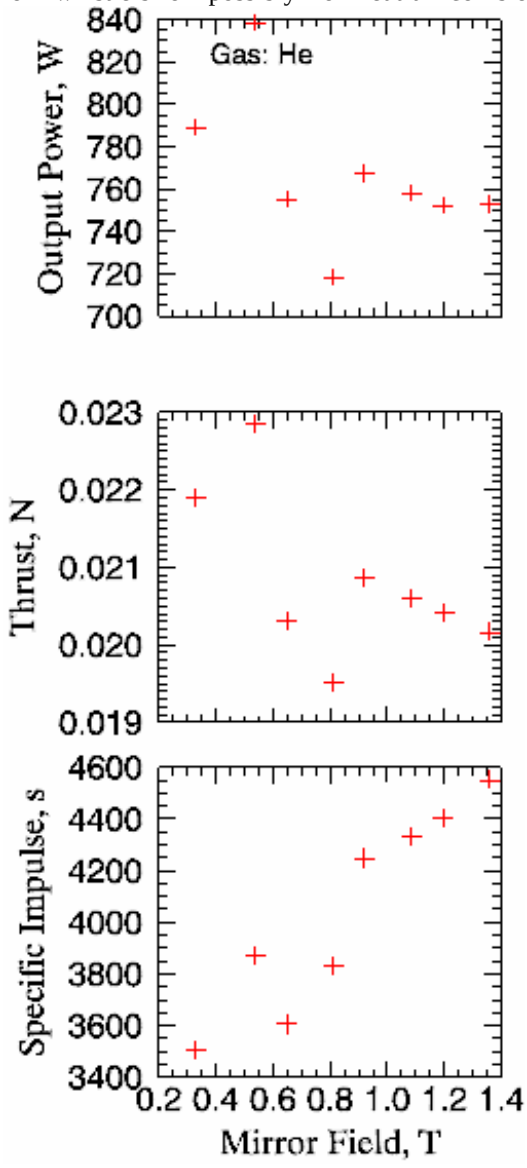

Figure 5. Power, thrust, and specific impulse inferred from the RPA data as a function of mirror magnetic field strength.

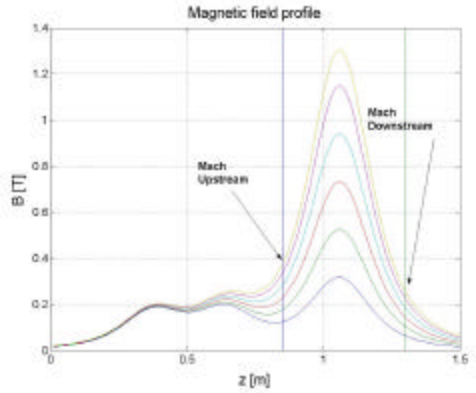

Figure 6. Magnetic field profile showing the location of the Mach probe measurements upstream and downstream of the magnetic mirror.

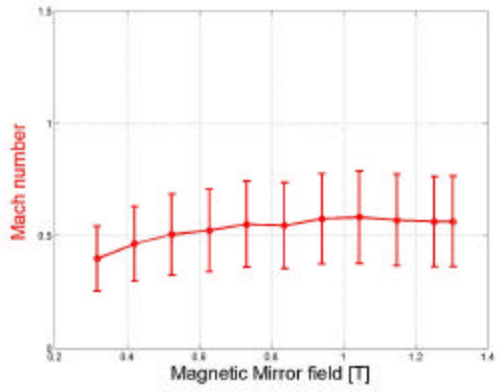

Figure 7. The Mach number measured upstream of the magnetic choke, corresponding to Figure 4.

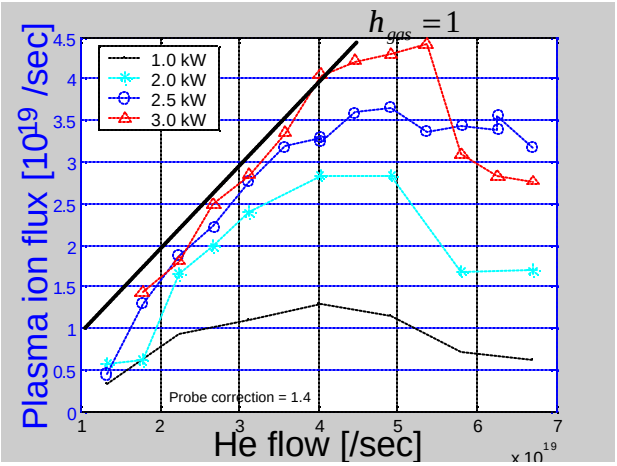

Figure 8. Output plasma ion flux plotted as a function of propellant input flow rate. The curves correspond to different levels of RF power input ot the helicon discharge.

centroid of the resulting ring distribution in phase space is not at 0, but at 8-10 km/s, indicating that the neutral flow speed may have been as high as 8-10 km/s

In another experiment, the ion velocity phase space distribution function was measured after installing the gas baffle and choke arrangement discussed above. As a result, the down stream neutral density has been reduced. Figure 10 shows the ion velocity phase space distribution obtained in this mode. The contrast of these results with Figure 9 is marked. Along the magnetic field, there is still a strong velocity phase space peak, in this case around 30-40 km/s. However, the distribution function is sharply confined to within 30° of the magnetic field, **B.** There was no evidence of a ring shaped distribution. The absence of the ring shaped distribution in the choked, low neutral pressure experiment is consistent with the ion-neutral scattering explanation and inconsistent with an ion whistler explanation for the ring distribution. This result is puzzling, since elastic collisions only preserve velocity in the center of mass frame, not the lab frame.

Ion Cyclotron Heating: Preliminary Results

Finally, we present the results of ICRF heating experiments from the summer of 2003. Two significant improvements in the ICRH configuration were installed during the spring of 2003 that allowed the achievement of useful plasma impedance on the ICRH antenna. These improvements were a larger diameter (9 cm), denser plasma discharge and a new transmitting antenna. The antenna is a double strap quarter turn configuration developed by our colleagues at Oak Ridge National Laboratory.

The effect of the ICRH heating is expected to be an increase in the component of the ion velocity perpendicular to the magnetic field. This increase will take place in the resonance region, i.e. the location where the injected RF wave frequency is equal to the ion cyclotron frequency. Downstream of the resonance, this perpendicular heating will be converted into axial flow owing to the requirement that the first adiabatic invariant of the particle motion be conserved as the magnetic field decreases. Since the total ion flux is not expected to increase, this axial acceleration should be accompanied by a density decrease. Furthermore, the particles should have a pitch angle distribution that does not peak at 0º. Instead, the distribution should peak at an angle that maps to a perpendicular pitch angle at resonance. Therefore a collimated detector oriented along the magnetic field should observe a decrease in total flux and an increase in particle energy. As the acceptance angle of the detector is increased, the ion saturation current should start to show an increase when the acceptance cone includes the peak in the pitch angle distribution.

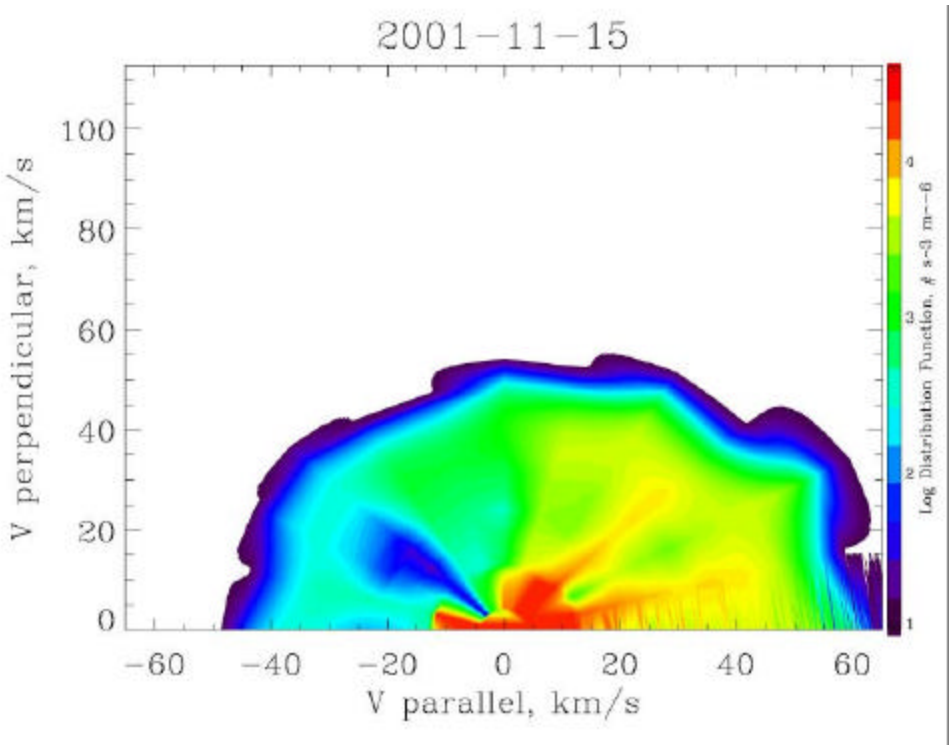

Figure 9. The velocity phase space distribution function of the VASIMR plasma during an experiment with the helicon in "unchoked" configuration. This mode results in high neutral pressure down stream and an ionization efficiency of about 50%.

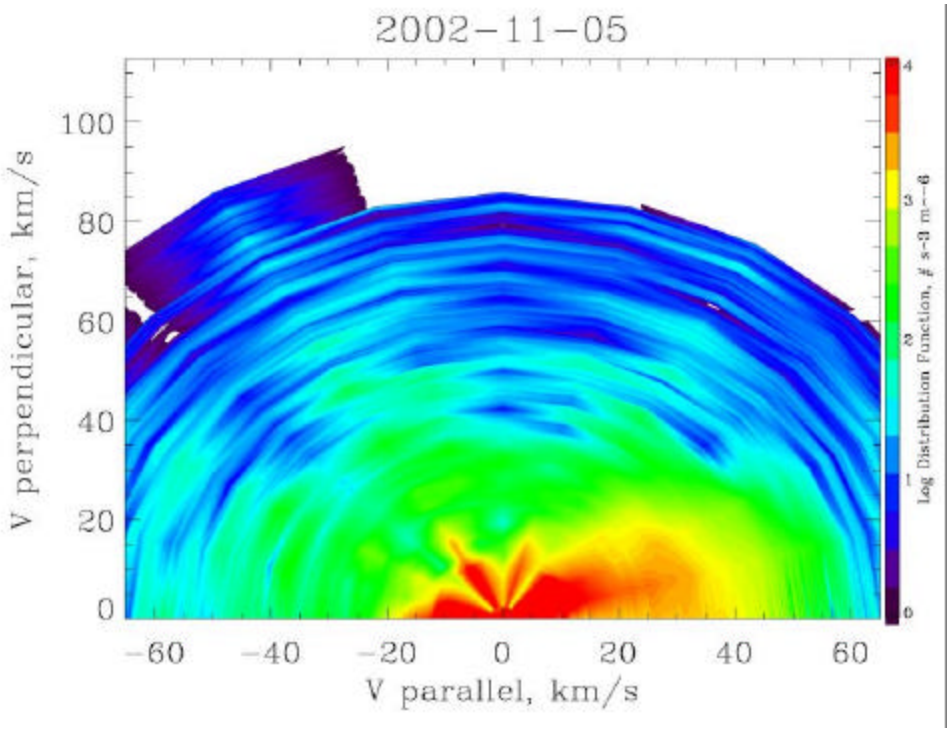

Figure 10. The velocity phase space distribution function of the VASIMR plasma during an experiment with the helicon in "choked" configuration. The choke and gas baffle act to confine the neutral gas within the helicon discharge. This mode results in a low neutral pressure down stream and an ionization efficiency of ~100%.

Three RPA configurations are available, tightly (2.5º) collimated, moderately (10º) collimated and effectively uncollimated (30º). The first two configurations are axially mounted and can be scanned along the axis of the engine. The third RPA can be rotated to any pitch angle and can be used to obtain 3-d pitch angle distributions. Figure 11 shows a comparison of the first derivative of the characteristic curve obtain by the wide aperture RPA during plasma shots run with and without ICRH. The upper, darker curve shows data taken during the ICRH shot. The elevated multi-peaked section between 50 and 130 eV is indicative of the presence of a population of strongly heated ions.

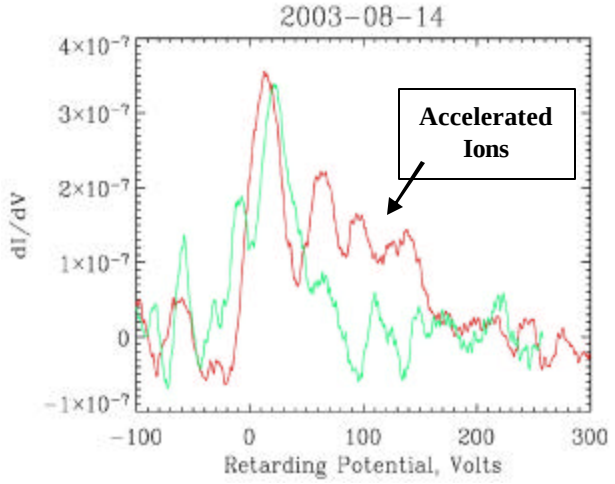

Figure 11. The first derivative of the current-voltage characteristics measured by an RPA with 30º collimation oriented at 10º pitch angle. The green curve shows a shot without ICRH, and the red curve shows a shot with ICRH.

The presence of what appears to be a hot component with low drift velocity is attributed to the fact that we have not yet been able to afford to obtain sufficient vacuum pumping capacity for this experiment. Consequently the background pressure builds up to at least 20 microtorr in the 50 cm region between the ICRH antenna and the RPA during the period of the discharge when RPA data were taken.

Figure 12 shows RPA ion current and ion energy distribution data taken by the highly collimated (2.5º) RPA looking along B. The darker, higher amplitude curves show data from a plasma shot with no ICRH. The lighter, low amplitude curves show data from a shot the same day, with the same magnetic field configuration and gas flow, with 1.5 kW of ICRH at 1.8 MHz applied.

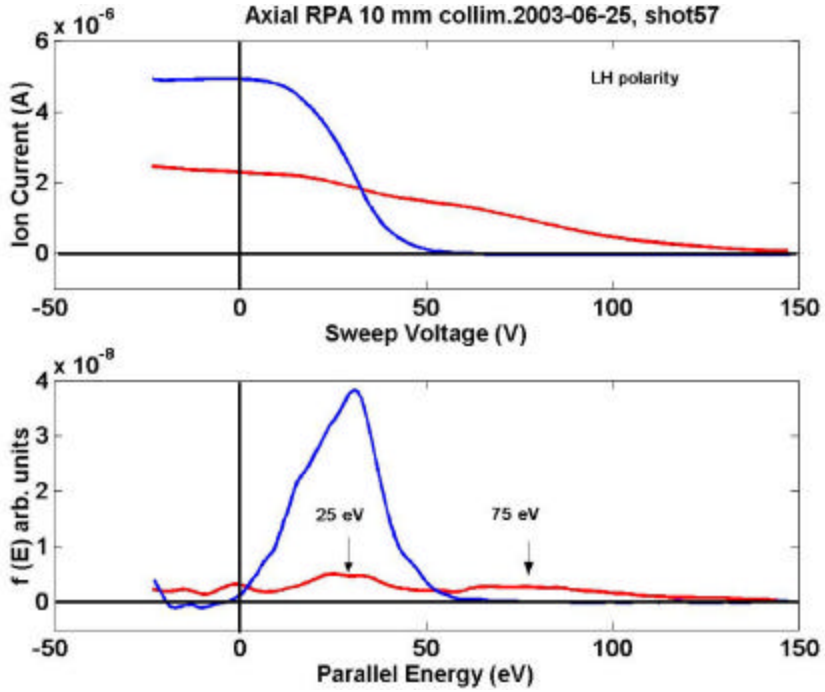

Figure 12. Top panel shows the current-voltage characteristics measured by an RPA with 2.5º collimation. The bottom panel shows the ion energy distribution in arbitraty units. The blue curve shows a shot without ICRH, and the red curve shows a shot with ICRH.

The data show exactly the expected signature. In contrast to the uncollimated RPA, and as expected, the current has been reduced by a factor of about two, while the ion energy shows a second peak with ~50 EV more energy than the plasma had prior to turning on the ICRH. Perhaps half the particles are in the accelerated component of the distribution, whereas half remain in (or have been thermalized back into) the lower energy component of the distribution.

The velocity phase space distribution functions corresponding to Figure 11 are found by dividing by the energy and are shown in Figure 13. The differences between the two curves appear less dramatic in this logarithmic presentation. Nonetheless, the effect of significant particle heating is apparent.

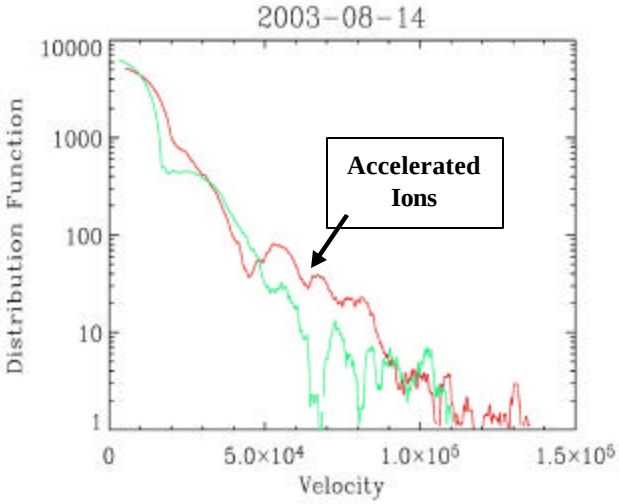

Figure 13. The ion velocity phase space distribution functions inferred from the data shown in Fig. 11.

The dynamic response of the plasma to the ICRH energy input has been studied by examining the temporal response of the plasma to brief bursts of ICRH transmission during individual shots. In order to simplify the plotting task, we have characterized the plasma during each voltage sweep of the retarding potential by least squares fitting a single component drifting Maxwellian to the RPA data. Figures 11-13 make clear that a single Maxwellian is a relatively poor approximation to the data. However, time variations in the inferred parameters do provide a general illustration of what was happening in the plasma.

Figure 14 shows an example of a time series plot obtained during a single shot. From top to bottom the panels show drift velocity, ion density, and ion temperature in the drifting frame. The wide aperture RPA oriented at 5º-pitch angle took these data. Three effects of the ICRH are apparent in the figure. Drift speed increased substantially, the density dropped and the temperature increased. All of the effects conform closely to the expected response to ICRH. Since, as will

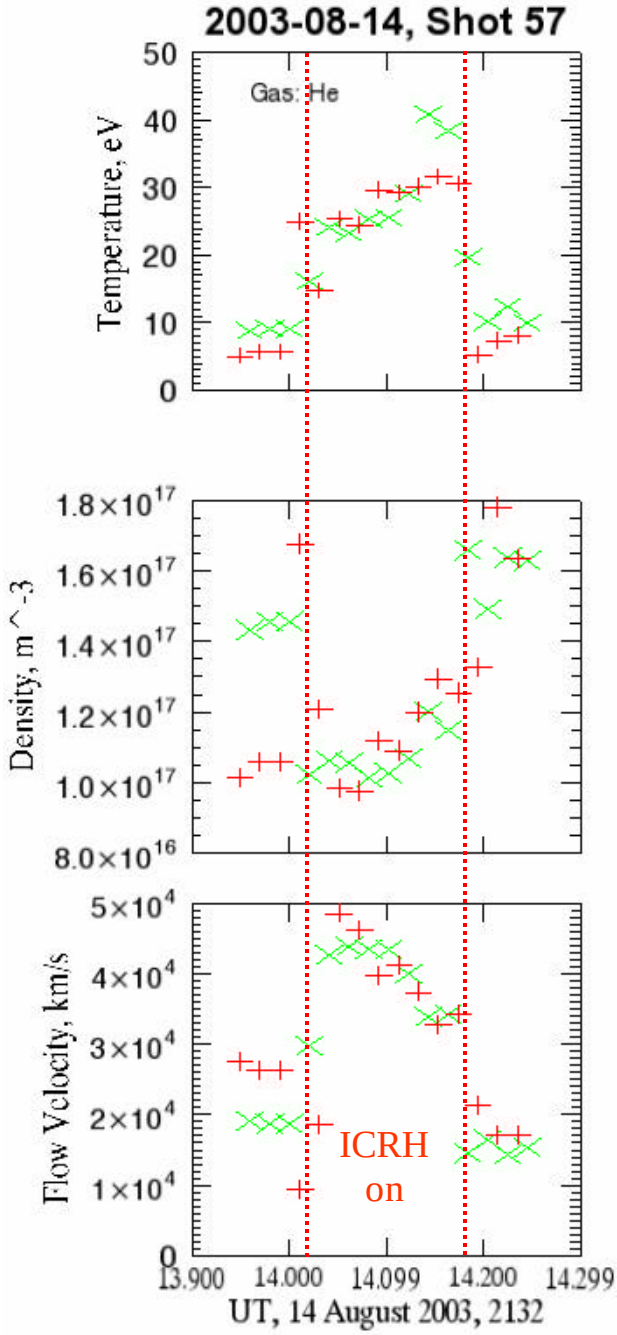

Figure 14. Fit parameters obtained by least squares fitting a drifting Maxwellian representation to each voltage sweep obtained by the wide angle RPA during a pulsed ICRH shot. From top to bottom, the panels show ion drift velocity, ion density and ion temperature in the frame of the beam. The plusses and X's show up and down sweeps. The vertical dashed lines show the times when the ICRH turned on and off.

be shown below, the single drifting Maxwellian is a poor approximation, the actual speed attained by the accelerated component is higher than the figure shows.

The full ion velocity phase space distribution function of the ions can be obtained by scanning the RPA in pitch angle, assuming cylindrical (gyrotropic) symmetry.

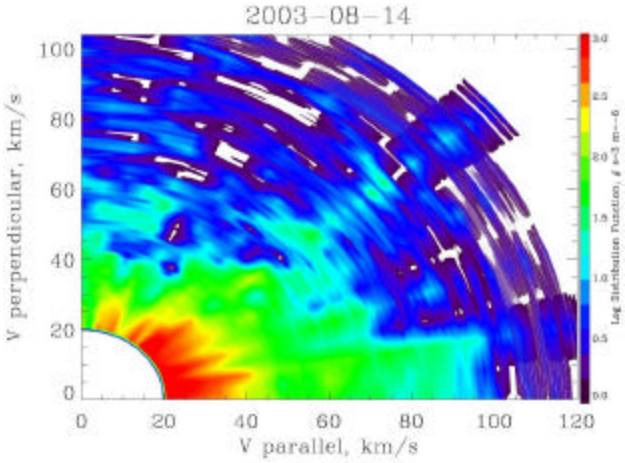

Figure 15. The ion velocity phase space distribution function obtained with ICRH on. The color bar scale is logarithmic. Note the intense 60-100 km/s ion jet at 10º-pitch angle.

An example of the distribution functions that have been observed during ICRH experiments is shown in Figure 15. During this particular experiment, the ICRH transmitter was operated at 1.85 MHz, at a power level of 1500 W. The data show a pronounced enhancement or jet of ions with v>60 km/s at 10º pitch angle. Although not particularly evident in the figure, detailed examination of the data show a depletion of ions with lower velocities and pitch angles.

As shown in Figure 2, the magnetic field intensity decreases rapidly with axial distance as one moves downstream away from the resonance region. At the location of the RPA's, the field strength is down by a factor of ~40 from the value at the cyclotron resonance point. In a region like this, the effects of conservation of the first adiabatic invariant dominate ion dynamics. What conservation of the first invariant does is to force particles to lower and lower pitch angles as the field strength drops. This mechanism is the basis for the magnetic nozzle that makes the VASIMR an attractive design concept in the first place. A particle's pitch angle is given by:

$$q = \arcsin\left(q_0 \sqrt{B / B_0}\right) \qquad (1)$$

A particle with a pitch angle of 90º at the resonance region will have a pitch angle of 10º at the location of the RPA. Thus all of the particles detected at ?>10º are either artifacts of the lack of collimation in the RPA or particles that have been scattered or charged exchanged.

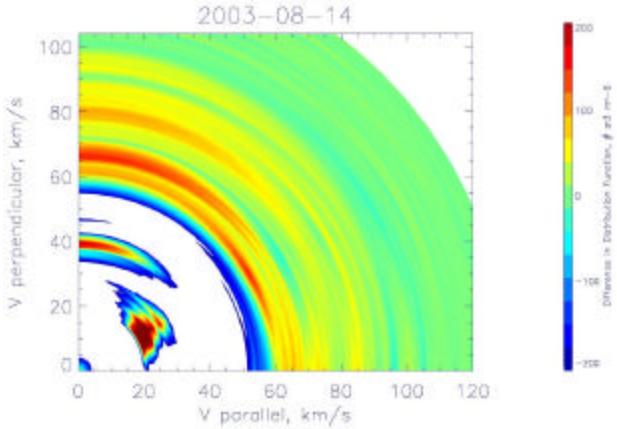

Figure 16. The difference in velocity phase space distribution function between ICRH on and ICRH off conditions plotted in spectrogram format using a linear color bar. The distribution has been mapped back to the location of cyclotron resonance using conservation of the first adiabatic invariant. The perpendicular heating effect of the ICRH shows up as the intense features at perpendicular velocities of 60-100 km/s.

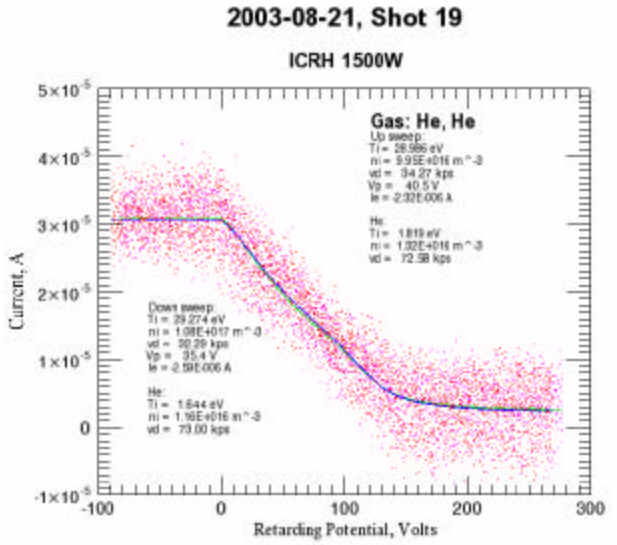

Figure 17. Raw RPA anode current plotted as a current-voltage characteristic. Data were obtained during an ICRH on shot. Solid lines show least-squares fits of drifting bi -Maxwellian representations, showing that the data can be modeled as the sum of a hot, slow component and a cold, fast component.

The effect of ion cyclotron heating on the exhaust plasma is perhaps best illustrated by subtracting the "ICRH off" distribution function from the "ICRH on" distribution function and mapping the result back to the resonance region (Figure 16). The results shown in Fig. 16 are very dramatic. There is a clear depletion of low energy ions and a significant enhancement of ions with perpendicular speeds >60 km/s, exactly as predicted for ICRH heating.

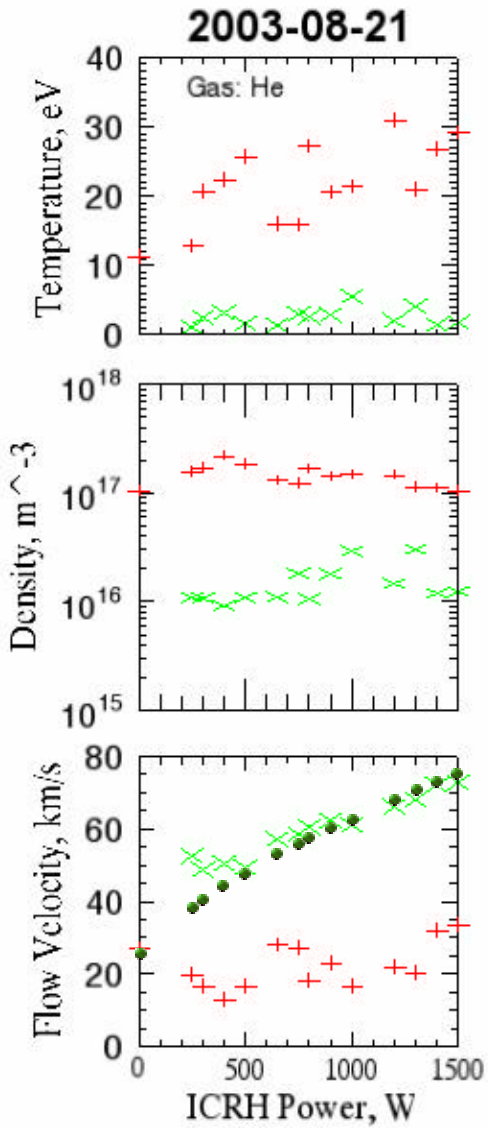

Figure 18. Fit parameters obtained by least squares fitting drifting bi-Maxwellian representations to the RPA data obtained during a scan of ICRH transmitter power. From top to bottom, the panels show ion drift velocity, ion density and ion temperature in the frame of the beam. The plusses show the slow, hot component. The X's show the fast, cold accelerated component. The round dots show the flow velocity expected for an energization rate of 70 eV/ion/kW of transmitted RF power.

The data in Figures 11-16 indicate that the high remaining neutral background pressure in the present VASIMR test chamber produces a substantial amount of resonant charge exchange and scattering between the ICRH antenna and the RPA location(s). The result is a pronounced "two-bump" distribution that is not well modeled by a single drifting Maxwellian. The data in Figure 12 strongly suggest using a bi-Maxwellian model consisting of a hot, slow component and a fast component that has a low temperature in the moving frame. An example of a bi-Maxwellian fit is shown in Figure 17.

The bi-Maxwellian model analysis has been used to interpret the results of a series of shots that scanned the ICRH power input from 0-1500 W. These results are presented in Figure 18. These results further strengthen the overall result of this paper, that the VASIMR VX-10 experiment is showing convincing evidence of single pass ICRF heating. The top panel shows that the accelerated beam has a low temperature in its reference frame, consistent with the expected output temperature of the helicon discharge. The temperature of the hot component is noisy. Generally it is much hotter than the helicon output is expected to be and the temperature increased with increasing ICRH power. The density of the accelerated component is 10-30% of the hot component, which is a measure of how much charge exchange and scattering is degrading the exhaust plume. We anticipate that the ratio of accelerated to scattered components will improve greatly with improved vacuum pumping capacity. The flow velocity of the cold, fast component increases as the square root of input power, almost exactly in agreement with the value predicted for an energization rate of 70 eV/ion/kW of transmitted power. It is important to note that the team has barely begun the process of optimizing antenna coupling, and a substantial improvement in this performance is expected in the near future.

CONCLUSIONS

The paper has presented a report on the present status of the development of the VASIMR engine. The paper has touched on a number of results, both scientific and technological. On the scientific side, our understanding of the physics of high power light-ion helicon discharges is growing steadily. On the technological side, we have seen a steady increase in the

plasma output and power efficiency of our helicon discharges. The helicon by itself is proving to be a reasonably effective thruster. We have begun to solve the problems of coupling the ICRH to the narrow and fast-moving output of the helicon discharge in a single pass. The best available data from several instruments and show that we have achieved strong perpendicular heating of the exhaust plasma ions. A heating rate of 70 eV/ion/kW of transmitted RF power has been observed, in good agreement with model predictions.

ACKNOWLEDGMENTS

NASA Johnson Space Center under grant NAG 9-1524, and the Texas Higher Education Coordinating Board under Advanced Technology Program project 003652-0464-1999 sponsored this research.

REFERENCES

[1] Chang Díaz F. R., "Research Status of The Variable Specific Impulse Magnetoplasma Rocket", *Proc. 39th Annual Meeting of the Division of Plasma Physics* (Pittsburgh, PA, 1997), Bulletin of APS, 42 (1997) 2057.

[2] Chang Díaz, F. R., "Research Status of The Variable Specific Impulse Magnetoplasma Rocket", Proceedings of Open Systems' July 27-31, 1998, Novosibirsk, Russia, *American Nuclear Society, Trans. of Fusion Technology*, 35 (1999) 87-93.

[3] Chang Díaz, F. R., Squire, J. P., Ilin, A. V., et al. "The Development of the VASIMR Engine", *Proceedings of International Conference on Electromagnetics in Advanced Applications (ICEAA99)*, Sept. 13-17, 1999, Torino, Italy, (1999) 99-102.

[4] Chang Díaz F. R., Squire J. P., Bering E. A. III, George J. A., Ilin A. V., Petro A. J. and Cassady L., "The VASIMR Engine Approach to Solar System Exploration", *Proceedings of 39th AIAA Aerospace Sciences Meeting and Exhibit'* Jan. 8-11, 2001, Reno, NV, AIAA 2001-0960 (2001)

[5] Chang Díaz, F. R., Squire, J. P., Bering, E.A. III, et al., "The VASIMR engine: Project status and recent accomplishments", *Proceedings of 42nd AIAA Aerospace Sciences Meeting and Exhibit'* Jan. 5-8, 2004, Reno, NV, AIAA 2004-0149 (2004).

[6] Boswell, R.W., *Phys. Lett. A 33* (1970) 457.

[7] Chen, F.F., *Plasma Phys. Controlled Fusion 33* (1991) 339.

[8] Golovato, S.N., Brau, K., Casey, J., et al., 'Plasma production and heating in a tandem mirror central cell by radio-frequency waves in the ion cyclotron frequency range', *Phys. Fluids 31* (1988) 3744.

[9] Yasaka, Y., Majeski, R., Browning, J., Hershkowitz, N., Roberts, D., 'ICRF heating with mode control provided by a rotating field antenna', *Nucl. Fusion 28* (1988) 1765.

[10] Chang Díaz, F.R., 'An Overview of the VASIMR Engine: High Power Space Propulsion with RF Plasma Generation and Heating', *Proceedings of Radio Frequency Power in Plasmas: 14th Topical Conference (Oxnard, California 2001)*, AIP Conference Proceedings 595, p. 3, Editors: T.K. Mau and J. deGrassie.

[11] Stix, T.H., *'Waves in Plasmas'*, (American Institute of Physics, New York 1992)

[12] Squire, J.P., Chang Díaz, F.R., Jacobson, V.T., McCaskill, G.E., Bengtson, R.D., Goulding, R.H., 'Helicon Plasma Injector and Ion Cyclotron Acceleration Development in the VASIMR Experiment', *Proceedings of 36th AIAA/ASME/SAE/ASEE Joint Propulsion Conference* (Huntsville, Alabama 2000) AIAA 2000-3752 (2000).

[13] Petro, A. J., Chang Díaz, F. R., Ilin, A. V., Squire, J. P., "Development of a Space Station-Based Flight Experiment for the VASIMR Magneto-Plasma Rocket," *Proceedings of 40th AIAA Aerospace Sciences Meeting and Exhibit* Jan. 14-17, 2002, Reno, NV, AIAA 2002-0344 .

[14] Chen, S., and Sekiguchi, T., "Instantaneous Direct-Display System of Plasma Parameters by Means of Triple Probe," *J. Appl. Phys.*, *36*(8), 2363-2375

[15] Stangeby, P.C., "Measuring Plasma Drift Velocities in Tokamak Edge Plasmas Using Probes," *Phys. Fluids.*, *27*(11), (1984) 2699-2704.

[16] Hutchinson, I.H., "Ion Collection by Probes in strong Magnetic Fields with Plasma Flow," *Phys. Rev. A*, *37*(11), (1988) 4358-4366.